the following reactions occurring in the reduction zone:

$$C + CO_2 \leftrightarrow 2\,CO \tag{9}$$

$$C + H_2O \leftrightarrow CO + H_2 \tag{10}$$

$$C + 2\,H_2 \leftrightarrow CH_4 \tag{11}$$

Eq. (9) and (10) can be combined in the whole shift reaction:

$$CO + H_2O \leftrightarrow CO_2 + H_2 \tag{12}$$

The equilibrium constant for methane formation, Eq. (11), and for the shift reaction, Eq. (12), can be written respectively as:

$$K_1 = \frac{P_{CH_4}}{(P_{H_2})^2} = \frac{x_5 \cdot n_{tot}}{x_1^2} \tag{13}$$

$$K_2 = \frac{P_{CO_2} \cdot P_{H_2}}{P_{CO} \cdot P_{H_2O}} = \frac{x_1 \cdot x_3}{x_2 \cdot x_4} \tag{14}$$

where P_i is the partial pressure of specie i, and $n_{tot} = \sum x_i$ is the total mole of the syngas. Equilibrium constants are function of the temperature and can be expressed by means the relation:

$$\ln K_p = \left(-\frac{\Delta G_T^o}{RT}\right) \tag{15}$$

where the standard Gibbs function of formation as function of the temperature is:

$$\Delta G_T^o = \Delta H_T^o - T\Delta S_T^o \tag{16}$$

In the above equation ΔH_T^o and ΔS_T^o are respectively the enthalpy and entropy change of the reaction. Values for standard Gibbs function and heat of formation at 298.15 K are collected in Table 1 for the different chemical species here involved. The dependence of the above functions by temperature was evaluated as proposed by the NIST by using data collected in the NIST Database. The general energy balance can be expressed as:

$$dH_{Biomass} + w dH_{H_2O_l} + \left(\frac{S}{B}\right)_{mol} dH_{Steam} + m\, dH_{O_2} + 3.76\, m\, dH_{N_2} = x_1 dH_{H_2} + x_2 dH_{CO} + x_3 dH_{CO_2} + x_4 dH_{H_2O_v} + x_5 dH_{CH_4} + (3.76\, m + c/2)\, dH_{N_2} \tag{17}$$

where $dH_{any\ specie}$ is the sum of the heat formation and the enthalpy change:

$$dH(T) = H_{f,298}^0 + \Delta H = H_{f,298}^0 + \int_{298}^{T} c_p(T)\, dT \tag{18}$$

The enthalpy change in the above equation can be evaluated by introducing the average specific heat over the temperature change defined as:

$$c_{p_{mh}} = R\left[A + BT_{am} + \frac{C}{3}(4T_{am}^2 - T_1T_2) + \frac{D}{T_1T_2}\right] \tag{19}$$

where $T_{am} = (T_1 + T_2)/2$ is the mean arithmetic temperature, A, B, C and D are the constants for any chemical species (Table 2) and R is the universal gas constant.

The heat of biomass formation was evaluated as proposed by [11] considering the follows ideal reactions:

$$C + O_2 \rightarrow CO_2 \quad \Delta H_c = -393509 \tag{20}$$

$$\frac{a}{2}H_2 + \frac{a}{4}O_2 \leftrightarrow \frac{a}{2}H_2O \quad \Delta H_c = \frac{a}{2}(-241818) \tag{21}$$

$$CO_2 + \frac{a}{2}\,H_2O \leftrightarrow CH_aO_b + \left(\frac{\frac{a}{2}-b+2}{2}\right)O_2$$
$$\Delta H_c = HHV_{Biom} \tag{22}$$

$$C + \frac{a}{2}\,H_2 + \frac{b}{2}O_2 \leftrightarrow CH_aO_b \quad \Delta H_f^0 = \sum \Delta H_{c,i} \tag{23}$$

Table 1. Gibbs energy function and standard heat of formation at 298.15 K

Chemical species	Phase	$\Delta G_{f\,298}^0$ [kJ/kmol]	$\Delta H_{f\,298}^0$ [kJ/kmol]
Carbon (Graphite), C	s	0.0	0.0
Carbon dioxide, CO_2	g	-394359	-393509
Carbon monoxide, CO	g	-137169	-110525
Hydrogen, H_2	g	0.0	0.0
Methane, CH_4	g	-50460	-74520
Oxygen, O_2	g	0.0	0.0
Water, H_2O	g	-228572	-241818
Water, H_2O	l	-237129	-285830

The system of non-linear equations was resolved by implementing them in an in-house code developed in Matlab®.

2.2 Syngas combustion model

Syngas from gasifier was fed in a post-combustion chamber where it was fully burned. Hot air from the micro turbine section was used as primary combustion air. A portion of cold exhaust gas was recycled to moderate the exit temperature of combustion gas.

Table 2. Heat capacity constants

Chemical species	T_{max} [K]	A	10^3 B	10^6 C	10^{-5} D
Carbon, C	2000	1.771	0.771	-	-0.867
Carbon dioxide, CO_2	2000	5.457	1.047	-	-1.157
Carbon monoxide, CO	2500	3.376	0.557	-	-0.031
Hydrogen, H_2	3000	3.249	0.422	-	0.083
Methane, CH_4	1500	1.702	9.081	-2.164	-
Oxygen, O_2	2000	3.639	0.506	-	-0.227
Water, H_2O	2000	3.470	1.450	-	0.121

Simple stoichiometric relations were used to evaluate the composition of exhaust gas while conservation of mass and energy were imposed to calculate the mass flow rate of the recycled gas for combustion temperature control. By considering syngas composition as input, the following reactions of combustion were considered:

$$CO + \frac{1}{2}\,O_2 + \frac{3.76}{2}N_2 \rightarrow CO_2 + \frac{3.76}{2}N_2 \tag{24}$$

$$H_2 + \frac{1}{2}\,O_2 + \frac{3.76}{2}N_2 \rightarrow H_2O + \frac{3.76}{2}N_2 \quad (25)$$

$$CH_4 + 2\,O_2 + 2\cdot 3.76N_2 \rightarrow CO_2 + 2H_2O + 2\cdot 3.76N_2 \quad (26)$$

Mass flow rate both for exhaust and recycled gas were calculated by imposing the conservation of mass and energy at the post-combustion chamber assumed as control volume in steady state conditions:

$$\dot{m}_{syn} + \dot{m}_{air,c} + \dot{m}_r - \dot{m}_{ex} = 0 \quad (27)$$

$$\dot{m}_{syn}dh_{syn} + \dot{m}_{air,c}dh_{air,c} + \dot{m}_r dh_r - \dot{m}_{ex}dh_r - \dot{Q}_{loss} = 0 \quad (28)$$

where $dh_{any\ mixture}$ is the enthalpy change calculated as in Eq. (18).

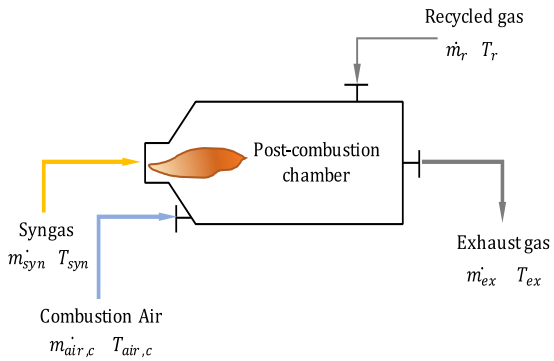

Figure 3. Post-combustion chamber scheme

Properties of the mixtures were calculated by using CoolProp® library once flue gas compositions were known. Thermal losses were imposed to be equal to 2% of the whole inlet thermal power.

2.3 Micro turbine thermodynamic model

Simple thermodynamic model was developed to get evaluations of the main cycle performances. Matlab® was used to implement the mathematical code by using CoolProp® libraries to evaluate fluid properties at each plant sections. With reference to the general scheme of the micro turbine section in regenerative mode depicted in Figure 2, air at conditions of temperature T_1 and pressure p_1, it is compressed by the compressor C1. Here an increase both in fluid pressure and temperature respectively to p_2 and to T_2 is performed. The compression work was evaluated as:

$$\dot{W}_c = \frac{\dot{m}_{air}\cdot(h_{2,is}-h_1)}{\eta_{is,c}\cdot\eta_{m,c}} \quad [W] \quad (29)$$

where $\eta_{is,c}$, $\eta_{m,c}$ are respectively the isentropic and the mechanical compressor efficiencies.

At the regenerator S2, the heat recovered by the hot air coming from the turbine exit section is used to preheat the same air at the compressor exit section. The recovered heat can be expressed as:

$$\dot{Q}_{S2} = (h_{2,1} - h_2) = (h_4 - h_{4,1}) \quad [W] \quad (30)$$

while that one subtracted at the evaporator S1 from the hot exhaust gases, as:

$$\dot{Q}_{S1} = \dot{m}_{ex}\cdot(h_{ex,in} - h_{ex,out}) = \dot{m}_{air}\cdot(h_3 - h_{2,1}) \quad [W] \quad (31)$$

Properties at the turbine T1 inlet section were evaluated once inlet temperature T_3 and pressure p_3 of the fluid were known, while the power produced was calculated by imposing the expansion ratio and the isentropic efficiency of the expander.

On the basis of the foregoing assumptions, the electrical power produced was evaluated as:

$$\dot{W}_{el} = \dot{m}_{air}\cdot(h_3 - h_{4,is})\cdot\eta_{is,t}\cdot\eta_{m,e}\cdot\eta_{el,g} \quad [W] \quad (32)$$

where $\eta_{is,t}$, $\eta_{m,e}$ are respectively the isentropic and the mechanical efficiencies of the expander, while $\eta_{el,g}$ is the electrical efficiency of the generator. On the basis of the previous calculations, the first law efficiency was then calculated as following:

$$\eta_I = \frac{\dot{W}_{el} - \dot{W}_c}{\dot{Q}_{S1}} \quad (33)$$

where required in the mathematical model, the difference of temperature between hot and cold fluids at regenerator S2 and at the evaporator S1, are fixed. This because in the first approach model developed here, there is no modelling of heat exchangers and so there is no prediction of fluid temperature at the exit sections of the heat exchangers. For the evaluation of the performances of the no regenerative layout, in the previous model it was simple imposed that $h_{2,1} = h_2$ so that:

$$\dot{Q}_{S1} = \dot{m}_{ex}\cdot(h_{ex,in} - h_{ex,out}) = \dot{m}_{air}\cdot(h_3 - h_2) \quad [W] \quad (34)$$

3. RESULTS

In this section, main results obtained by mathematical models previously presented are given and discussed in some details. To get a better comprehension of the influence of each operational parameter at sub-system level on the whole plant performances, results by each sub-model are discussed separately. First results by biomass gasification model are analysed in terms of the effects of the main process parameters (mainly biomass moisture and gasification equivalence ratio) on syngas composition, LHV, syngas production rate and gasification cold efficiency. Therefore, follows the micro turbine cycle analysis where the effects of the compression ratio and the inlet turbine temperature on the thermodynamic cycle performances, both for regenerative and no regenerative layout, are discussed. At least the global plant performances are presented in term of the first law efficiency. Main results obtained by the equilibrium gasification model are summarized and presented in the following figures. Simulations were carried out by considering almond shells as biomass. Ultimate analysis and caloric properties are shown in Table 3. The equations presented in sections 2.1 were resolved here by considering the ER (i.e. the air mass flow rate), the biomass composition (and so its moisture), the steam to biomass ratio S/B (in the calculations equal to zero, i.e. no additional water other than moisture in the biomass was considered) as main input parameters of the problem. Clearly, in this formulation, the gasification temperature is an unknown of the mathematical problem.

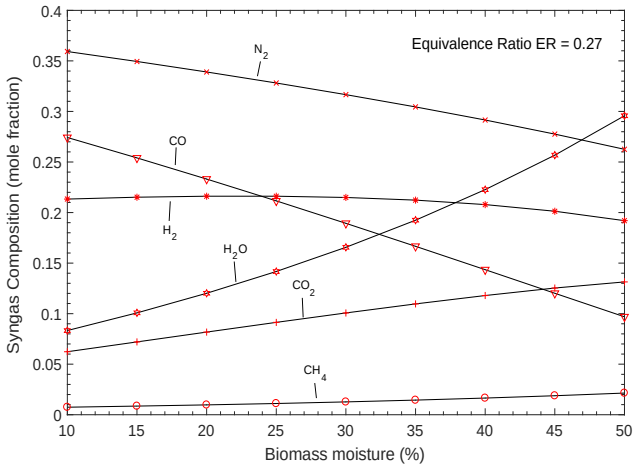

(a)

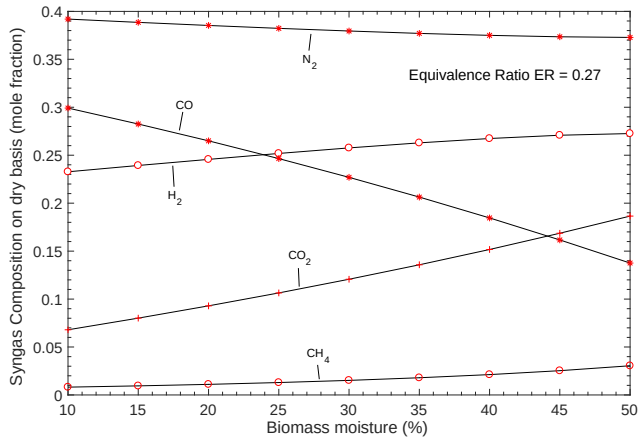

(b)

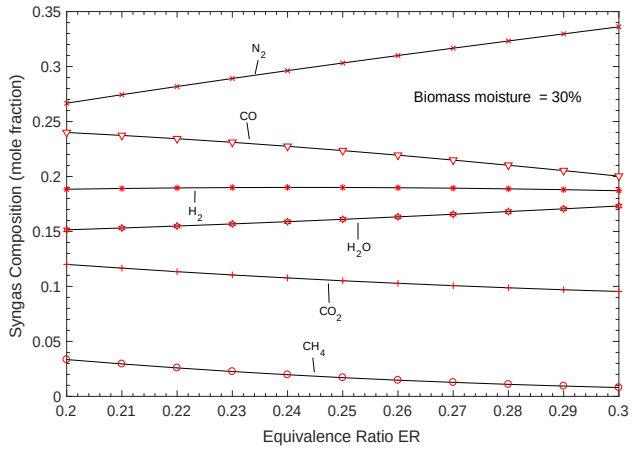

(c)

Figure 4. Syngas composition as function of the biomass moisture at constant equivalence ratio on wet (a) and dry basis (b) and as function of the equivalence ratio at constant biomass moisture (c)

Figure 4 (a) and (b), respectively referred to syngas wet and dry basis, show the effect of biomass moisture on syngas composition.

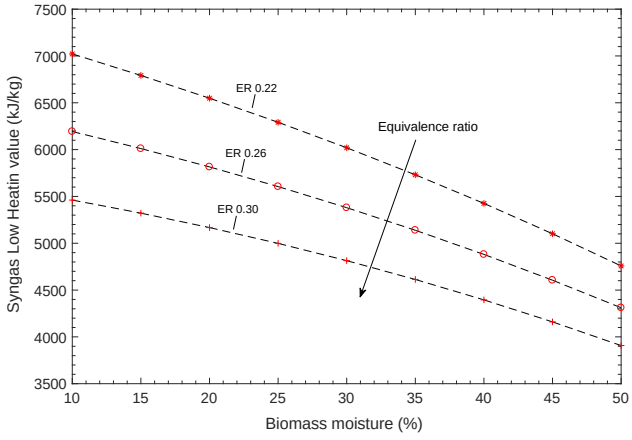

(a)

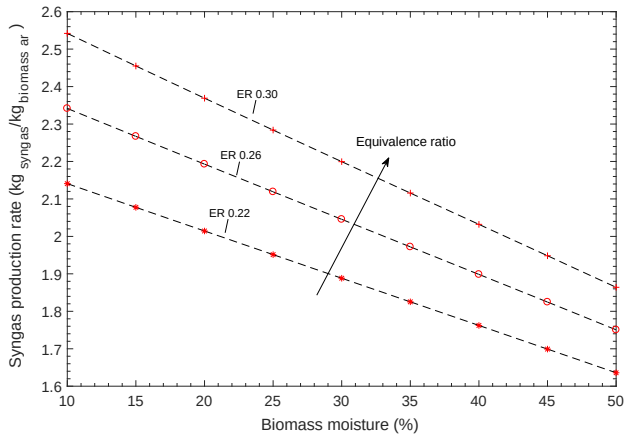

(b)

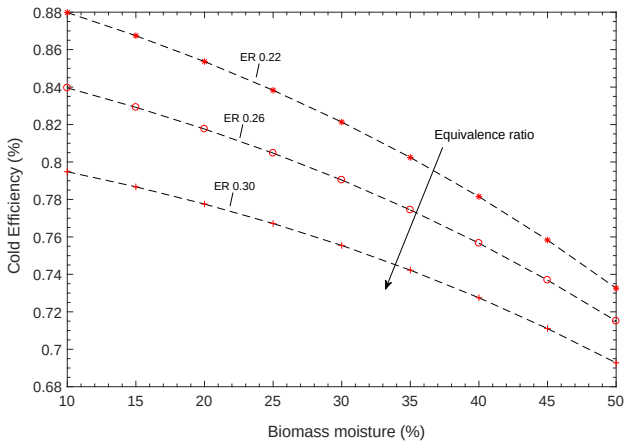

(c)

Figure 5. Syngas low heating value (a), syngas production rate (b) and gasification cold efficiency (c) as function of the biomass moisture and equivalence ratio

As it can be observed, methane concentration is very low: in all cases analysed, below 3% in mole fraction if referred to dry syngas composition. As biomass moisture increase, hydrogen and methane (this latter in less marked way) contents slightly increase as expected. A similar trend is observed for the carbon dioxide. On the contrary, carbon monoxide monolithically decreases about by the same percentage witch water increases. This is also explicable by the increase in carbon dioxide. Nitrogen content instead, is constant as

expected (at constant equivalence ratio no more nitrogen is introduced inside the gasifier). At least, Figure 4-(c), shows the influence on syngas composition of the gasification equivalence ratio at constant biomass moisture content (30% in the case analysed).

Table 3. Ultimate analysis for biomass material (dry basis, weight percentage), low heating value and moisture of as received matter. Data from ENEA analysis

Biomass	% (w/w dry)					
	C	H	N	O	S	Ashes
Almond shells	48.9	6.2	0.18	43.5	0.026	1.65

Biomass	LHV [MJ/kg$_{db}$]	Moisture [% w/w]
Almond Shells	17.89	13.8

As can be noted, as the equivalence ratio increases, all combustible molecules (i.e. hydrogen, methane and carbon monoxide) tend to decrease while, on the contrary, nitrogen increases (much more oxygen is available for combustion reactions and much more nitrogen is introduced in the gasifier with air). This, in last instance, its traduces in a decrease of both in syngas low heating value and in plant cold efficiency as showed in Figure 5 (a) and (c) respectively. On the contrary, due the greater amount of air introduced in the system, syngas production rate increases too, Figure 5-(b).

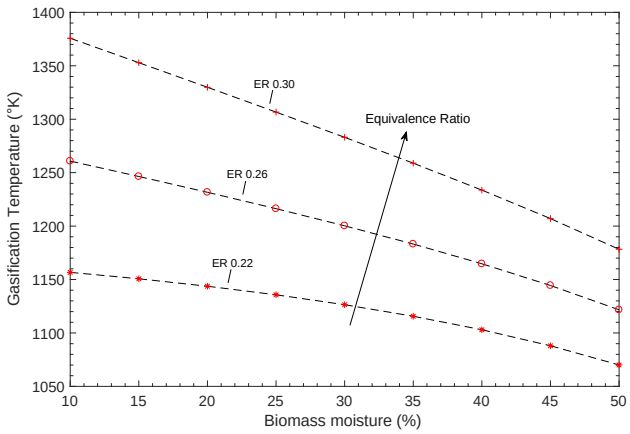

Figure 6. Gasification temperature as function of the biomass moisture and equivalence ratio

The gasification temperature, Figure 6, increases as the biomass moisture decreases and the equivalence ratio increases. This because, in the first case (moisture decrease) more heat is available to be stored in the form of syngas sensible heat, while in the second latter (ER increase), higher temperatures are reached as consequence of the greater amount of combustible molecules burned (much more air is introduced in the gasifier).

Though the true model validation is beyond the purpose of the present work, as reference, in Table 4 experimental data for syngas composition by downdraft gasifier are collected by different authors. As can be noted, the range of variability is very high because of the dependence of syngas composition by a great number of gasifier work conditions and by biomass composition. Anyway, theoretical data obtained by model seem to be in good agreement with experimental ones.

Table 4. Experimental syngas composition from downdraft gasifier. Data collected by different works as reported by [13-15] and confirmed by the thirty years' experience of the ENEA in the gasification field

Properties	Range (dry basis)
LHV (MJ/Nm^3)	4.0 – 5.6
H_2 (vol %)	15 – 21
CO (vol %)	10 – 22
CO_2 (vol %)	11 – 13
CH_4 (vol %)	1 - 5
C_nH_m (vol %)	0.5 – 2
N_2 (vol %)	Remaining

Main results by micro turbine thermodynamic model are collected in Figure 6, where the influence of the compression ratio and the maximum turbine inlet temperature (TIT) on both cycle first law efficiency and specific work are presented. Data showed are referred to the real thermodynamic cycle behaviour. In the same figure, comparisons between regenerative (grey line) and simple configurations (red line) are presented. As expected, specific work and thus cycle efficiency, both increase as TIT increases. In all cases a maximum is reached for increasing compression ratio as higher is TIT. Such a condition in more evident for simple configuration while for the regenerative one, a nearly independence from compression ratio is observed. In this latter case, maximum is reached in the neighbourhood of $\beta_c = 2$. For the regenerative configuration, at given TIT, efficiency decreases as pressure ratio increases because of the decreased amount of heat internally regenerated. As shown, regeneration results a thermodynamically beneficial practice up to a certain value of the compression ratio (β_{lim}) above witch the efficiency is slightly lower than that evaluated for the simple cycle.

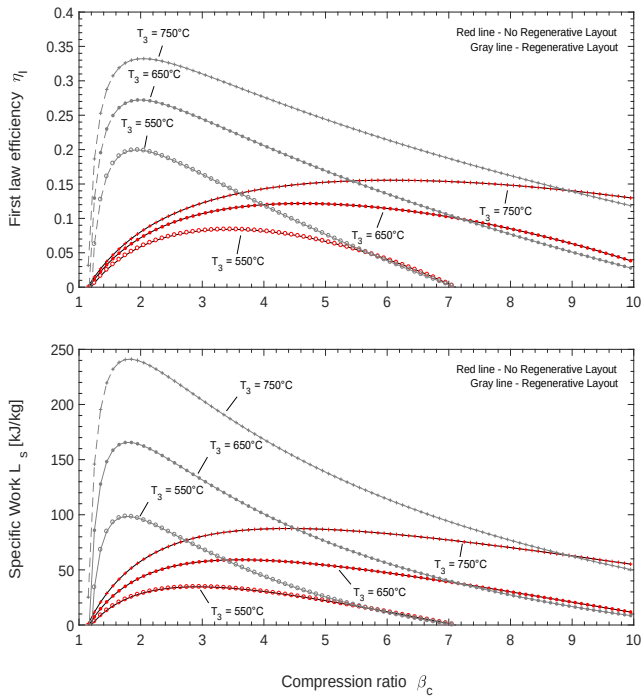

Figure 7. First law efficiency and specific work as function of the compression ratio and the inlet turbine temperature

Figure 7 and Figure 8 show, respectively for the simple (i.e.

Figure 1) and the regenerative (i.e. Figure 2) plant configurations, the first law efficiency as function of the TIT and the compression ratio at the micro-turbine section.

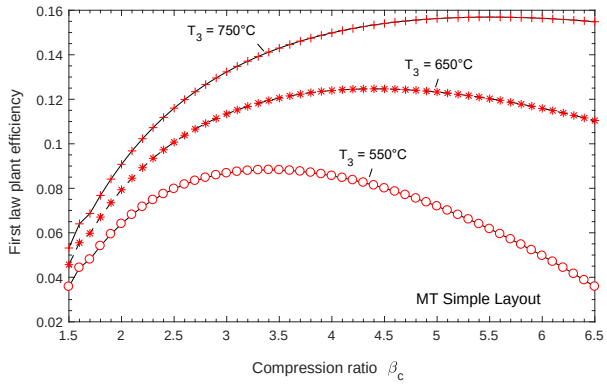

Figure 7. First law efficiency for the simple plant configuration as function of the compression ratio and the inlet turbine temperature

Gasification parameters (i.e. biomass composition and moisture as in Table 3, ER = 0.26) as well as the post-combustion temperature (Tex = 850 °C) were kept constant. Main theoretical results at each plant sections as function of the same parameters considered above at the MT, were collected for the regenerative configuration in Table 5. As expected, plant efficiency exhibits a similar trend respect to that of the MT cycle. Also in this case a maximum in plant efficiency was reached approximatively where MT cycle efficiency has a maximum.

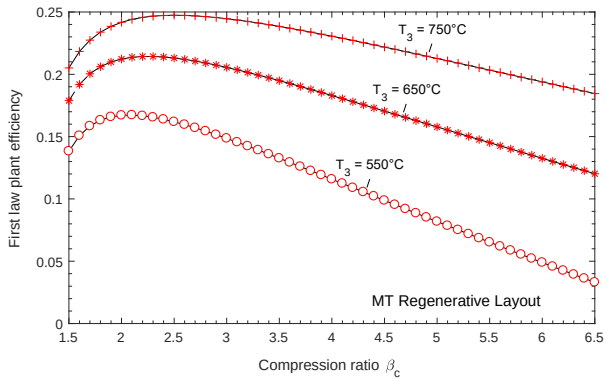

Figure 8. First law efficiency for the regenerative plant configuration as function of the compression ratio and the inlet turbine temperature

As can be noted, plant efficiency for the regenerative configuration is always higher than simple configuration with a peak of about 25% at TIT 750 °C and β_c close to 2.5. Nevertheless, for those cases where efficiency exceeds 20%, it must be noted that the temperature at the over-heater S1 hot side outlet section, is on average higher than 450 °C. This means that expensive plant solutions (i.e. high temperature cleaning systems and blowers or alternatively regenerative combustion chamber for the purpose designed) should be adopted. All this could be not economically feasible for small scale applications. Alternatively, simple plant configuration must be considered. In this latter case, acceptable efficiencies (in the order of 16%) can be reach at TIT 750°C and β_c close to 4.5. The challenge is now the high TIT.

Table 5. Main theoretical results by the whole numerical model developed for the regenerative plant configuration

Regenerative plant configuration as shown in Figure 2							
Gasification parameters		**Compression Ratio at MT Compressor**					
		3,5		4,5		5,5	
ER	0,26	**TIT (°C)**					
Moisture	13.8%	650	750	650	750	650	750
Mass flow rate (kg/h) :							
Gasifier							
Biomass IN		89,8	71,4	102,7	76,1	120,6	82,2
Gasification Air IN		115,3	91,6	131,7	97,5	154,6	105,4
Syngas OUT		205,3	163,1	234,7	173,8	275,5	187,8
Ashes OUT		0,090	0,071	0,103	0,076	0,121	0,082
Post-Combustion chamber							
Syngas IN		205,3	163,1	234,7	173,8	275,5	187,8
Recycled gas IN		1741,2	1786,3	1876,8	1729,5	2121,7	1757,9
Combustion Air IN		361,5	287,2	413,4	306,2	485,7	331,0
Exhaust gas OUT		2308,0	2236,6	2524,8	2209,5	2882,9	2276,7
Exhaust gas at CH01		566,8	450,3	648,1	479,9	761,2	518,8
Micro Turbine							
AIR IN		4584,3	3051,7	4693,3	2923,4	5142,4	2956,7
Temperature (°C) :							
Gasifier							
Gasification AIR IN		192,2	187,1	236,6	231,7	273,9	269,3
Syngas OUT		968,3	967,1	979,2	978,0	988,5	987,3
Post-Combustion chamber							
Syngas IN		968,3	967,1	979,2	978,0	988,5	987,3
Recycled gas IN		438,6	535,4	401,4	493,9	373,2	462,5
Combustion Air IN		192,2	187,1	236,6	231,7	273,9	269,3
Exhaust gas OUT		850,0	850,0	850,0	850,0	850,0	850,0
Micro Turbine							
Air IN T_1		20,0	20,0	20,0	20,0	20,0	20,0
Compressor OUT T_2		189,3	189,3	229,6	229,6	263,8	263,8
S2 Cold side OUT		423,6	520,4	386,4	478,9	358,2	447,5
T_3 (TIT)		650,0	750,0	650,0	750,0	650,0	750,0
Turbine OUT - T_4		438,6	535,4	401,4	493,9	373,2	462,5
S2 Hot side OUT T_{41}		192,2	187,1	236,6	231,7	273,9	269,3
S1 Hot side OUT		438,6	535,4	401,4	493,9	373,2	462,5
Main plant performances :							
Q_1 at S1 [kW_{th}]		334,2	250,5	396,8	278,7	479,9	311,4
P_{el} [kW_{el}]		75,0	75,0	75,0	75,0	75,0	75,0
η_{cold}		0,831	0,831	0,832	0,832	0,833	0,833
$\eta_{I,MT}$		0,236	0,315	0,199	0,283	0,165	0,254
$\eta_{I,plant}$		0,195	0,245	0,170	0,230	0,145	0,213

4. CONCLUSION

In this study, a solution where syngas by downdraft gasifier is directly burned to feed an externally fired air turbine was introduced and numerically analysed. Mathematical model of the whole power system was developed by using MatLab® and by implementing CoolProp® library for fluids properties evaluations. Two configurations identified as simple and regenerative were thus compared in terms of the first law efficiency. Results showed that appreciable improvements in plant efficiency can be achieved by using regenerative

configuration alternatively to simple one. Nevertheless, expensive equipment solutions should be considered to meet the high temperature fluids conditions (greater than 450°C) at the hot side outlet of the over-heater heat exchanger S1. All this makes this configuration supposedly inapplicable for small scale power generation unless to develop alternative and cheaper solutions for the regenerative heat exchanger (i.e. by enclosing the combustion chamber, the high temperature heat exchanger S1 and the recycling line all in one equipment). Simple layout surely allows for lower efficiencies (in the order of 16%) if compared to the regenerative one by using a simpler plant arrangement in terms of utilities and maximum temperatures involved (now the fluid temperature at the hot side outlet of S1 is in the order of 230 ° C). Furthermore, also in this case, TIT in the order of 750 °C requires attentions.

REFERENCES

[1] Tapas KP, Nimisha KR, Pratik NS. (2016). A comprehensive dynamic model for downdraft gasifier using heat and mass transport coupled with reaction kinetics. Energy 116: 1230-1242. https://doi.org/10.1016/j.energy.2016.10.036

[2] Prakashbhai RB, Raymond LH, Ajay K, Sunil T, Natarianto I. (2018). Scale-up of a downdraft gasifier system for commercial scale mobile power generation. Renewable Energy 118: 25-33. https://doi.org/10.1016/j.renene.2017.11.002

[3] Susastriawana A, Saptoadi H, Purnomo. (2017). Small-scale downdraft gasifiers for biomass gasification: A review. Renewable and Sustainable Energy Reviews (76): 989-1003. http://dx.doi.org/10.1016/j.rser.2017.03.112

[4] González FOC, Mahkamov K, Lora EES, Andrade RV, Jaen RL. (2013). Prediction by mathematical modeling of the behavior of an internal combustion engine to be fed with gas from biomass, in comparison to the same engine fueled with gasoline or methane. Renewable Energy 60: 427-432.https://doi.org/10.1016/j.renene.2013.05.037

[5] Parthasarathy NKP. (2014). Hydrogen production from steam gasification of - biomass: Influence of process parameters on hydrogen yield – a review. Renewable Energy 66: 570-579. https://doi.org/10.1016/j.renene.2013.12.025

[6] Pedroso DT, Machin EB, Pérez NP, Bollini L, Silveira BJL. (2017). Technical assessment of the Biomass Integrated Gasification/Gas Turbine Combined Cycle (BIG/GTCC) incorporation in the sugarcane industry. Renewable Energy 114: 464-479. https://doi.org/10.1016/j.renene.2017.07.038

[7] Din ZU, Zainal ZA. (2016). Biomass integrated gasification–SOFC systems: Technology overview. Renewable and Sustainable Energy Reviews 53: 1356-1376. https://doi.org/10.1016/j.rser.2015.09.013

[8] Nakamura S, Yoshikawa K. (2016). Biomass gasification process with the tar removal technologies utilizing bio-oil scrubber and char bed. Applied Energy 170: 186-192. https://doi.org/10.1016/j.apenergy.2016.02.113

[9] Roy PC, Datta A, Chakraborty N. (2013). An assessment of different biomass feedstocks in a downdraft gasifier for engine application. Fuel 106: 864-868. https://doi.org/10.1016/j.fuel.2012.12.053

[10] Chaves LI, Silva MJ, Souza SNM, et al. (2016). Small-scale power generation analysis: Downdraft gasifier coupled to engine generator set. Renewable and Sustainable Energy Reviews 58: 491-498. https://doi.org/10.1016/j.rser.2015.12.033

[11] Zainal ZA, Ali R, Lean CH, Seetharamu KN. (2001). Prediction of performance of a downdraft gasifier using equilibrium modeling for different biomass material. Energy Conversion and Management 42: 1499-1515.

[12] Jia J, Xu L, Abudula A, Sun B. (2018). Effects of operating parameters on performance of a downdraft gasifier in steady and transient state. Energy Conversion and Management 155: 138-146. http://dx.doi.org/10.1016/j.enconman.2017.10.072

[13] Couto N, Rouboa A, Silva V, Monteiro E, Bouziane K. (2013). Influence of the biomass gasification processes on the final composition of syngas. Energy Procedia 36: 596-606. https://doi.org/10.1016/j.egypro.2013.07.068

[14] Kirsanovs V, Blumberga D, Veidenbergs I, Rochas C, Vigants E, Vigants G. (2017). Experimental investigation of downdraft gasifier at various conditions. Energy Procedia 15: 332-338.

[15] Il Son Y, Jun Yoon S, Ku Kim Y, Goo Lee J. (2011). Gasification and power generation characteristics of woody biomass utilizing a downdraft gasifier. Biomass Bioenergy 35: 4215-4220. https://doi.org/10.1016/j.biombioe.2011.07.008

NOMENCLATURE

Ash	Biomass ashes content [% wt]
$c_{p_{mh}}$	Average specific heat [kJ/kmol K]
$\Delta G^0_{f\ 298}$	Standard Gibbs function at 298.15 K [kJ/kmol]
$dH_{any\ specie}$	Sum of the heat formation and the enthalpy change [kJ/kmol]
HHV_{Biom}	Biomass High Heating Value [kJ/kmol]
$H^0_{f,298}$	Standard heat of formation at 298.15 K [kJ/kmol]
ΔH^o_T	Enthalpy change of reaction at T [kJ/kmol]
K	Equilibrium constant
LHV_{Biom}	Biomass Low Heating Value [kJ/kmol]
m	Total oxygen reacted [kmol]
M	Mass [kg]
MC	Moisture content [% wt]
PM	Molecular weight [kg/kmol]
$\dot{Q}$	Thermal power rate [W]
R	Universal gas constant (8.314 J/mol K)
ΔS^o_T	Entropy change of reaction at T [kJ/kmol K]
TIT	Temperature at turbine inlet
w	Total water reacted [kmol]
$\dot{W}$	Mechanical power rate [W]
$x_1..x_5$	Stoichiometric coefficients [kmol]

Greek symbols

β_c	Compression ratio
η_I	First law efficiency
η_c	Gasification cold efficiency

Subscripts

air	Air
Biomass $_{ar}$	Biomass As Received
Biomass $_{daf}$	Biomass Dry-Ash-Free
c	Compressor
e	Exit
el	Electrical
H_2O	Water